

Influence of Temperature Variations on Calibrated Cameras

Peter Podbreznik, Božidar Potočnik

Abstract—The camera parameters are changed due to temperature variations, which directly influence calibrated cameras accuracy. Robustness of calibration methods were measured and their accuracy was tested. An error ratio due to camera parameters change with respect to total error originated during calibration process was determined. It pointed out that influence of temperature variations decrease by increasing distance of observed objects from cameras.

Keywords—camera calibration, perspective projection matrix, epipolar geometry, temperature variation.

I. INTRODUCTION

A pilot project for real-time activity tracking on the building site was developed. An application can automatically recognize differences between as-planned and as-built from building site images [7]. Application concept is based on comparison between real-time captured images and 4D model, made by 4D tool [8]. On the building site a temporary equipment (e.g. scaffolding stage, panellings) is the part of the building object during building process. Some parts of buildings are because of temporary equipment out of camera field of view. For this reason, the building site images should be captured from multiple cameras, with fixed positions and orientations. Joining multiple cameras views is possible, if multiple camera system setup is calibrated. Camera calibration can be performed by various methods like: eight-point algorithm, LMedS, RANSAC, M-estimators [1], [3], [11].

Calibrated cameras are often used for many different tasks, where they are exposed to different environmental variations, e.g. temperature variations. Calibrated low-cost CCD cameras were used in geodetic devices for distance measuring [4]. The measured distance error was 8 mm/°C [4]. Thermal low-cost CCD cameras were analyzed and small deviation of intrinsic camera parameters was detected in [9].

Cameras on the building site are exposed to different weather conditions and, thus, their accuracy is truncated, because of intrinsic and extrinsic camera parameters changes [6]. A change of extrinsic camera parameters commences due to changes of geometrical properties of bearing structure with mounted camera. Bearing structure actually expands due to temperature variations. In the other hand, a change of intrinsic camera parameters appears as a result of change of optical system geometric properties. For known bearing structure and temperature variations, the error magnitude for particular camera (i.e. observed point deviation from predicted point) can be calculated on image plane in pixel units.

This error for particular camera directly influences calibrated cameras and corresponding points determination. In general, the error of calibrated cameras emerges, because of following reasons: (i) numerical error of calibration method,

(ii) inaccurate determination of initial corresponding points (ICP), and (iii) camera parameters changes due to temperature variations. Individual errors are merged into total error magnitude, which presents deviations for corresponding points.

Cameras on the building site are usually influenced by temperature variations, therefore, the focus of this paper is on error estimation due to temperature variations for calibrated cameras. First, the robustness of calibrated methods were tested and their accuracy was measured. Afterwards, the above-mentioned reasons were analyzed and the error ratio, because of temperature variations, was estimated with respect to the total error magnitude of calibrated cameras. Statements were confirmed with logical conclusions and experimental measurements.

This paper consists of six sections. In Section 2, an analytical camera model, influenced by temperature variations, is described, followed by a review of calibration methods and measurement of their robustness in Section 3. Section 4 analyses temperature influence on calibrated cameras. Results are presented and explained in Section 5. This paper concludes with some suggestions for future work.

II. ANALYTICAL CAMERA MODEL SUPPLEMENTED WITH INFLUENCE OF TEMPERATURE VARIATIONS

Spatial objects are projected on image plane by camera. This transformation is described with analytical camera model, as follows:

$$\mathbf{p} = \frac{1}{z} \mathcal{M} \mathbf{P}, \quad (1)$$

where z is distance between normalized image plane and camera, \mathbf{p} is projected point of spatial point \mathbf{P} , and \mathcal{M} is perspective projection matrix, defined as:

$$\mathcal{M} = \mathcal{K} \begin{pmatrix} \mathcal{R} & \mathbf{t} \end{pmatrix}. \quad (2)$$

Matrix \mathcal{K} is calibration matrix, \mathcal{R} is rotation matrix, and \mathbf{t} is translation vector [1], [2]. Calibration matrix \mathcal{K} determines intrinsic camera parameters, while matrix \mathcal{R} and translation vector \mathbf{t} describes extrinsic camera parameters [1], [2], [11].

A. Perspective projection matrix \mathcal{M}_T

Analytical camera model, supplemented by influence of temperature variations, is described by matrix \mathcal{M}_T as [6]:

$$\mathcal{M}_T = \begin{pmatrix} f_\alpha \mathbf{r}_1^T + s \mathbf{r}_2^T + u_0 \mathbf{r}_3^T & f_\alpha t_{T_x} - s t_{T_y} + u_0 t_{T_z} \\ f_\beta \mathbf{r}_2^T + v_0 \mathbf{r}_3^T & f_\beta t_{T_y} + v_0 t_{T_z} \\ \mathbf{r}_3^T & t_{T_z} \end{pmatrix}, \quad (3)$$

where \mathbf{r}_1^T , \mathbf{r}_2^T , and \mathbf{r}_3^T are rows of rotation matrix \mathcal{R} ; t_{T_x} , t_{T_y} , and t_{T_z} are components of translation vector \mathbf{t}_T ; while parameters f_α , f_β , u_0 , v_0 , and s are intrinsic camera parameters. Translation vector \mathbf{t}_T is calculated as:

$$\mathbf{t}_T = \mathbf{t}_{T_0} + \Delta \mathbf{t}_{T_r},$$

where \mathbf{t}_{T_0} is translation vector at normal temperature ($T_0 = 20^\circ\text{C}$) and $\Delta \mathbf{t}_{T_r}$ is variation of translation vector due to temperature variations ΔT . Perspective projection matrix alters above all due to variation of vector $\Delta \mathbf{t}_{T_r}$ [6].

III. OVERVIEW OF CAMERA CALIBRATION METHODS

Relations between two camera views can be established by using their parameters. In general, camera parameters are unknown and relation between cameras should be established by epipolar geometry [1], [2], [11]. Such geometry requires information about initial corresponding points (ICP) for mathematical determination of fundamental matrix \mathcal{F} . Linear eight-point algorithm is basic calibration method. It assures good results if ICP points are well selected (i.e. ICP precisely determined and well distributed on image). If ICP points are not selected well enough then robust calibration methods should be used. M-estimator method, least median of squares (LMedS), and RANSAC are the most appropriate methods for camera calibration [11]. The most applicable calibration method are surveyable described in this sequel.

A. Linear eight-point algorithm

Linear methods are sensitive to input data (i.e. ICP points). Inappropriate determined ICP (e.g. points too close to each other, wrong relations between ICP points) provoke false calculation of fundamental matrix \mathcal{F} . Such matrix is, of course, not suitable to establish relations between two camera views.

Observed point \mathbf{P} is spatial point; \mathbf{O} and \mathbf{O}' are optical camera centers; and images Π and Π' contain projected observed point \mathbf{p} and \mathbf{p}' . Equation

$$\mathbf{p}'^T \mathcal{F} \mathbf{p} = 0 \quad (4)$$

determines relation between projected point \mathbf{p} and \mathbf{p}' , defined by fundamental matrix \mathcal{F} . Above equation can be rearranged as:

$$(u', v', 1) \begin{pmatrix} F_{11} & F_{12} & F_{13} \\ F_{21} & F_{22} & F_{23} \\ F_{31} & F_{32} & F_{33} \end{pmatrix} \begin{pmatrix} u \\ v \\ 1 \end{pmatrix} = 0, \quad (5)$$

and can be rewritten in short form as:

$$\mathbf{w}^T \mathbf{f} = 0, \quad (6)$$

where:

$$\mathbf{w} = [u'u, u'v, u', v'u, v'v, v', u, v, 1]^T$$

and

$$\mathbf{f} = [F_{11}, F_{12}, F_{13}, F_{21}, F_{22}, F_{23}, F_{31}, F_{32}, F_{33}]^T. \quad (7)$$

We can derive from equations (6) and (7) the following form:

$$\begin{aligned} & u'uF_{11} + u'vF_{12} + u'F_{13} + \\ & v'uF_{21} + v'vF_{22} + v'F_{23} + \\ & uF_{31} + vF_{32} + F_{33} = 0. \end{aligned} \quad (8)$$

Belonging ICP points from both images represent one row in matrix \mathcal{A} (see equation (9)). To obtain fundamental matrix we must solve a system with nine unknowns and nine equations. Because this system is homogenous, the value F_{33} can be set to 1 and the system still has a uniform solution. Eight ICP points, appearing in pairs $\mathbf{p}_i \leftrightarrow \mathbf{p}'_i$ ($i = 1, \dots, 8$), suffice to uniformly solve this system. These pairs actually fills up the 8×8 homogeneous system of linear equations:

$$\mathcal{A} \mathbf{f} = 0. \quad (9)$$

In general, the eight-point algorithm requires n pairs of ICP. For $n = 8$ the system has uniform solution. However, if $n > 8$ ICP pairs are used, then more accurate fundamental matrix \mathcal{F} is obtained.

Usually, a normalization of ICP pairs is carried out to improve fundamental matrix estimation. This procedure has two steps. In the first step, ICP points are translated so that their centroid is at origin. Afterwards, the points are scaled so that their average distance from origin is $\sqrt{2}$. Translation and scale matrix are merged into transformation matrix \mathcal{T} . Normalized points are then used in system given by equation (9).

The most convenient way to solve the system with m equations and n unknowns, where $m > n$, is singular value decomposition method (SVD). Matrix \mathcal{A} by using SVD is obtained as:

$$\mathcal{A} = \mathcal{U} \mathcal{S} \mathcal{V}^T, \quad (10)$$

where \mathcal{U} and \mathcal{V} are orthogonal matrices and $\mathcal{S} = \text{diag}(r, s, t)$ is diagonal matrix satisfying $r \geq s \geq t$.

The matrix \mathcal{A} is, thus, composed of matrices \mathcal{U} , \mathcal{S} , and \mathcal{V} , where the last column of matrix \mathcal{V} is a solution and vector \mathbf{f} , respectively (see equation (7)). Afterwards, the 3×3 fundamental matrix \mathcal{F}'' is constructed from vector \mathbf{f} .

Singularity is important properties of fundamental matrix, but the matrix \mathcal{F}'' does not satisfied it in general [2]. For this reason, a new matrix \mathcal{F}' is established as:

$$\mathcal{F}' = \mathcal{U} \text{diag}(r, s, 0) \mathcal{V}^T,$$

where \mathcal{F}' is singular matrix having rank 2.

Obtained solution is based on normalized ICP points, thus, matrix \mathcal{F}' has to be renormalized with transformation matrices from both images, i.e. matrices \mathcal{T} and \mathcal{T}' , by equation

$$\mathcal{F} = \mathcal{T}'^T \mathcal{F}' \mathcal{T}. \quad (11)$$

Matrix \mathcal{F} is singular fundamental matrix which enables restoration of relations between points $\mathbf{p}_i \leftrightarrow \mathbf{p}'_i$ on images from both camera views.

Linear method is very sensitive to noise and errors in ICP points, which reflect in inaccurate fundamental matrix. Robust method should be used, if ICP contains points with wrong positions or incorrectly determined relations.

B. M-estimators

Let ICP points be given and r_i denotes a difference of i -th point from its correct position. Method minimizing an expression $\sum_i r_i^2$ in the least-square sense, becomes unstable,

if ICP points contains outliers. In this case, minimization procedure damages the fundamental matrix which becomes useless. Metod M-estimators tries to decrease influence of outliers by changing a square function in minimization with more appropriate function ρ . A modified minimization now reads:

$$\min \sum_i \rho(r_i), \quad (12)$$

where ρ is positive symmetric function with unique minimum [11]. Function ρ can be determined with different influence functions like: L_2 , L_1 , $L_1 - L_2$, L_p , "Fair", Huber, Cauchy, Tukey. In this research, the "Fair" influence function ρ was used, defined as:

$$\rho(x) = c^2 \left[\frac{|x|}{c} - \log\left(1 + \frac{|x|}{c}\right) \right],$$

where c is constant [10].

Equation (12) is solved by multidimensional minimization. The Nelder-Mead simplex algorithm was used in this research [5].

C. Least Median of Squares – LMedS

This method estimates fundamental matrix by nonlinear minimization of expression:

$$\min \text{median } r_i^2,$$

where minimum r_i from the median of squared residuals, computed for the entire set of ICP, must be found. The solution is obtained by time consuming searching of problem space. Searching is speed up by randomly selecting patterns from ICP points, where each pattern consists of k pairs of ICP. Quality of solution depends upon number of patterns, i.e. m . Optimal number of patterns results in lower computation time and well estimated fundamental matrix \mathcal{F} . Let suitable pattern contains k (pairs) of well established ICP points. Let us presume that a ratio of incorrectly established pairs in ICP is ε . Then, a probability that at least one out of m patterns is well established, is defined as:

$$P = 1 - \left[1 - (1 - \varepsilon)^k \right]^m. \quad (13)$$

From desired probability P , where k and ε are given, the number of patterns m can be calculated.

D. RANSAC

The RANSAC method searches for minimal number of randomly selected patterns, which will credible represent ICP points [11]. Still acceptable error value should be known a priori to test matching of selected patterns with entire population. Method idea and implementation are very similar as in method LMedS. The main differences are:

- threshold for acceptable error value expressed in pixels is determined manually, and
- method LMedS calculates median of squared differences, while RANSAC counts ICP pairs within acceptable error threshold. A pattern with this minimal number, contains the maximal number of well established ICP pairs.

IV. INFLUENCE OF TEMPERATURE VARIATIONS ON CALIBRATED CAMERAS

The analytical camera model was supplemented by a term for measuring variations of extrinsic camera parameters in [6]. The equation for error magnitude calculation for observed objects was derived. Calculation combines (i) the distance r between camera and observed object and (ii) temperature variation ΔT with respect to temperature during camera calibration. Obtained error magnitude or deviation, denoted as N , is expressed in pixels. It pointed out that error magnitude of camera on building site due to temperature variations is less than pixel. Our findings were confirmed with experiments [6].

A. Influence of external temperature variations on camera calibration procedure

Temperature variations influence each camera and its corresponding bearing structure, independent of camera system. The total error magnitude of calibrated cameras due to temperature variations has to be determined. We describe the influence of temperature variations on calibrated cameras with two statements:

- Statement 1: Two cameras are calibrated at arbitrary temperature and then, at the same temperature provoke the error by searching corresponding points. This error has a same magnitude as is numerical error of calibration method (i.e. errors in Table I, where both criteria are zero).
- Statement 2: Cameras are calibrated at temperature T which is different as normal temperature ($T_0 = 20^\circ\text{C}$) and corresponding points are searched at normal temperature. Then, the error of calibrated cameras is the same as, if we will calibrate cameras at the normal temperature with ICP points, which are altered by error magnitude due to temperature variations ΔT ($\Delta T = T_0 - T$).

Proofs of both statements are based on logical conclusions and are presented in this sequel.

Influence of temperature variations on camera was analyzed in [6]. Image actually changes only, if extrinsic camera parameters are altered. This alternation is result of temperature expansion of camera bearing structure for vector Δt_{T_r} at direction of construction vector \mathbf{v}_s [6]. Statements 2 is based on the fact, that it is irrelevant, if camera is translated in direction \mathbf{t} or if observed object is moved for vector $-\mathbf{t}$. On this way, variations of extrinsic camera parameters, due to temperature variations, can be treated as deviation or ICP translation. The distance of observed object from camera, i.e. r , and temperature change with respect to temperature at camera calibration, i.e. ΔT , have to be known to calculate ICP translation.

B. Influence of external temperature variations on corresponding points searching

Difference between temperatures, when the cameras were calibrated T_c and used T_u (i.e. by searching corresponding points), must be determined. Besides, the variation of translation vector Δt_{T_r} , must be calculated for each camera as

follows:

$$\Delta t_{T_r} = t_{T_c} - t_{T_u}, \quad (14)$$

where t_{T_c} is a translation vector during camera calibration and t_{T_u} is a translation vector during corresponding points searching.

An error magnitude is estimated by using statement 2. Statement 2 actually presupposes that positions of ICP points are incorrect for error magnitude, originated due to temperature variations. Error of ICP points is not randomly distributed, but direction and size are known and are the same for all ICP points for particular camera. If ICP points of both cameras contain the same error magnitude and direction (i.e. the same translation vector Δt_{T_r}), then this error is not reflected. Namely, just difference between vectors $\Delta t_{T_{r1}}$ and $\Delta t_{T_{r2}}$ is important:

$$\Delta t = \Delta t_{T_{r2}} - \Delta t_{T_{r1}}, \quad (15)$$

where $\Delta t_{T_{r1}}$ and $\Delta t_{T_{r2}}$ are alterations of translation vectors of first and second camera, respectively. Fig. 1a depicts a situation, where vectors $\Delta t_{T_{r1}}$ and $\Delta t_{T_{r2}}$ are the same. Their difference Δt is then zero vector.

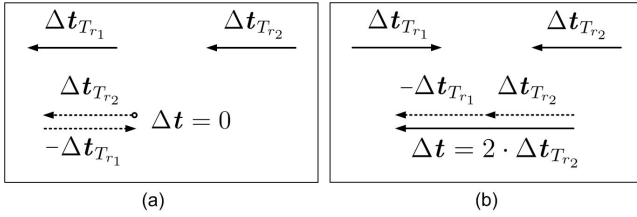


Fig. 1. Difference, denoted as Δt , between alteration of translation vector for the second camera, $\Delta t_{T_{r2}}$, and alteration of translation vector for the first camera, $\Delta t_{T_{r1}}$: a) both vectors have the same size and the same direction; b) both vectors have opposite directions and the same size.

The equation (15) enables a transfer of extrinsic camera parameters error from both cameras to the one camera only. Thus, the first camera can be considered faultless, while the second camera contains (accumulated) error of extrinsic camera parameters, provoked due to translation Δt . Difference of translation vectors Δt must then be transformed from length units to pixels (procedure was explained in [6]). Calculated error is added up within error emerged during calibration process (i.e. numerical error of calibration method and inaccurate positions of ICP points). Finally, a total error N of two calibrated cameras is determined as:

$$N = N_c + N_u, \quad (16)$$

where N_c is error emerged during calibration process and N_u is error, arisen due to variations of camera parameters as consequence of temperature variations [6].

1) *Error analysis for the eight-point algorithm*: Eight-point algorithm is a basic calibration method and is used also in robust calibration methods like LMedS, RANSAC, and M-estimators. To estimate error analytically, we must supplement an eight-point algorithm (see Section III-A) by error model term, similarly as we did for individual camera in [6]. This error is reflected as:

- error in ICP points, which are used in calibration process and
- inaccuracy of corresponding points positions during estimation of correspondence between the first and the second image.

ICP points directly determine values of matrix \mathcal{A} . The key role in calibration has a method for solving equation system. In this research, the SVD method was used. Used SVD method has the following properties:

- method becomes unstable, if ICP points are very close to each other [11]. Therefore, equally distributed points from entire image have to be chosen; and
- equations system is pre-determinate, i.e. usually more than eight ICP points are used for fundamental matrix \mathcal{F} calculation.

Equation system solution directly depends on choice and number of ICP points, which are determined either manually or automatically. Therefore, a system numerical stability cannot be a priori assured. Pre-determinate equation system (and its eventual instability) does not assure unique solution. Analytical determination of error originated during two cameras calibration is, thus, not possible.

An error of corresponding points, denoted as N_c , was, therefore, experimentally determined for each calibration method.

2) *Relative ratio of camera parameters error due to temperature variations*: Total error N is calculated by using equation (16). It appears because of (i) numerical error of calibration method, (ii) inaccurate ICP points, and (iii) variations of camera parameters due to external temperature variations.

Relative error ratio due to camera parameters variations, denoted as N_{u_r} , is determined with respect to the total error N like:

$$N_{u_r} = \frac{N_u}{N}. \quad (17)$$

Camera parameters variations depend merely on temperature variations, thus, initial temperature is not important. It was shown in [6] the size of observed object decreases, measured in pixel, when distance from observed object to the camera increases. Each pixel, therefore, covers larger surface on observed object. By "enlarging" pixel size, an camera error N_u is decreased and, consequently, its relative error ratio in total error N .

V. RESULTS

Robustness of four calibration methods, i.e. eight-point algorithm, LMedS, RANSAC, and M-estimators, was tested in this paper.

An accuracy of M-estimators method depends on input data (i.e. initial vectors). For this reason, two versions of this method were tested: (i) method M-estimators*, where input data were obtained directly from linear eight-point algorithm, and (ii) method M-estimators**, where input data were calculated by using LMedS method. Robustness of these methods was tested and measured on various set of ICP points. Results are presented in Table I. Calibration method error N_c and relative error ratio N_{u_r} originate due to temperature variations were calculated. All together 100 pairs of manually

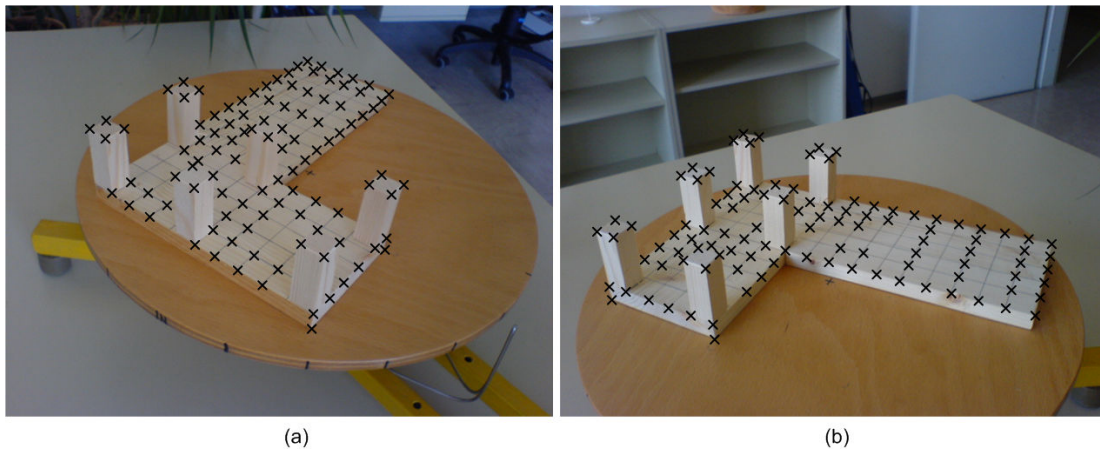


Fig. 2. Experimental environment: a) first camera view and b) second camera view. Small crosses denote manually determined ICP. All together 100 pairs of ICP points were available.

determined error-free ICP points were available for calibration. Actual input data sets of ICP used in calibration process were constructed from this error-free ICP set by deliberately corrupting some of ICP pairs. Two criteria were used for corrupting ICP pairs (see Table I): (i) vertical criteria denotes a percentage of corrupted ICP pairs in input data set, (ii) horizontal criteria denotes a magnitude of ICP pairs corruption. Magnitude of ICP pairs corruption was defined as percentage with respect to expression $\frac{H+W}{2}$, where H and W are image height and width expressed in pixels, respectively. The vertical criterion is shortly denoted as "% of corrupted ICP pairs", while horizontal criterion is abbreviated as "position error of ICP pairs in %". Two test images, with size of 640×480 pixels, are depicted in Fig. 2. Images were related with 100 manually established ICP pairs. Individual calibration method was tested on various input data sets. Each criterion is splitted into six classes (+ error-free class). Each method was, thus, tested with 36 different input data sets. Twenty measurements were performed for every input data set. Deviations of ICP points from their real positions were, then, calculated. Average deviations are presented in Table I. These deviations are actually calibration methods error N_c .

From Table I is evidently, that method LMedS is applicable, if input data set contains small percentage of corrupted ICP pairs also with large position errors. The same consideration is true for method RANSAC, which is very similar to LMedS method (see Section III-D). The opposite is true for M-estimators* method. This method is robust for data set with high percentage of corrupted ICP pairs, where each point is corrupted just for small magnitude. The method M-estimators** is insensitive on small and large errors. The reason is in input data set, which was obtained by robust LMedS method. With such combination of methods, we obtain a calibration method, which is on one side robust to small position errors also at high percentage of corrupted ICP pairs, and on the other side is robust to small percentage of corrupted ICP pairs also for big position error (see Table I, M-estimators** method).

Accuracy of calibrated cameras depends on selection of

ICP points and their accurate position. Inaccuracy of ICP points appears mainly in manual or automatic proces of their selection. Error of camera calibration method, N_c , can be estimated by using results from Table I. Corresponding measurement should be read, for specific method and with respect to the used input data set, which depends on two criteria:

- expected percentage of corrupted ICP points (vertical) and
- expected magnitude of position error of ICP points (horizontal).

Interpreting results from Table I on such way the actual error N_c of calibrated cameras is obtained. This error does not include error due to temperature variations.

Difference of translation vector Δt (arisen due to temperature variations) provokes camera translation (see Section IV-B). For known distance r from observed object to the camera, it is possible on image to estimate error N_c originated due to camera parameters variations. Total error N of calibrated cameras can be calculated from partial errors N_c and N_u by using equation (16).

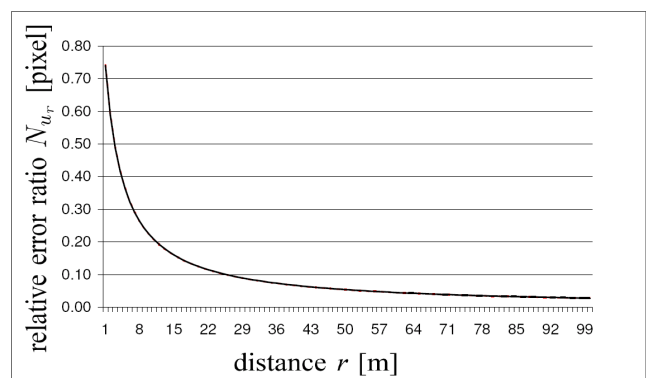


Fig. 3. Relative error ratio due to camera parameters variations, $N_{u,r}$, with respect to the distance r .

Fig. 3 depicts relative error ratio due to camera parameters

TABLE I

CALIBRATION METHOD ERROR N_c EXPRESSED IN PIXEL. DIFFERENT INPUT DATA SET OF ICP WAS USED. CRITERION "% OF CORRUPTED" DETERMINES A PERCENTAGE OF CORRUPTED ICP POINTS FROM ENTIRE DATA SET WITH ERROR POSITION, WHILE CRITERION "POSITION ERROR" DETERMINES MEAGNITUDE OF THIS POSITION ERROR. EACH INPUT DATA SET CONTAINS 100 ICP PAIRS.

Linear eight-point algorithm								
		position error of ICP pairs in %						
		0	10	20	30	40	50	70
% of corrupted ICP pairs	0	3.871	-	-	-	-	-	-
	5	4.735	7.644	15.064	19.155	26.714	37.533	
	10	5.169	9.851	19.202	27.830	37.872	71.424	
	20	6.835	14.533	28.043	43.461	56.976	83.333	
	30	7.306	18.749	40.041	62.833	68.354	75.726	
	40	8.210	20.508	41.946	68.960	74.940	92.945	
	50	9.420	24.976	53.607	62.723	77.889	83.348	

LMedS								
		position error of ICP pairs in %						
		0	10	20	30	40	50	70
% of corrupted ICP pairs	0	1.056	-	-	-	-	-	-
	5	1.778	3.383	4.227	6.132	7.233	11.190	
	10	3.059	6.120	12.131	12.270	16.896	18.321	
	20	5.162	11.643	17.176	26.154	31.893	33.313	
	30	6.824	15.717	28.938	35.293	39.602	42.618	
	40	9.057	20.794	36.431	44.382	50.486	55.510	
	50	11.372	27.712	40.574	49.602	53.588	57.249	

RANSAC								
		position error of ICP pairs in %						
		0	10	20	30	40	50	70
% of corrupted ICP pairs	0	1.903	-	-	-	-	-	-
	5	2.787	1.998	3.828	7.588	15.793	14.553	
	10	6.209	10.974	17.338	20.083	27.568	21.788	
	20	16.395	30.628	41.264	50.870	44.922	46.021	
	30	24.083	38.058	42.949	56.228	55.042	44.715	
	40	33.876	37.176	63.328	58.660	73.399	72.063	
	50	33.833	45.270	62.919	81.365	86.729	85.400	

Method M-estimators* (initial vectors obtained by eight-point algorithm)								
		position error of ICP pairs in %						
		0	10	20	30	40	50	70
% of corrupted ICP pairs	0	1.234	-	-	-	-	-	-
	5	2.700	6.791	10.005	14.156	24.037	30.364	
	10	3.455	8.747	19.930	24.703	33.851	43.539	
	20	4.704	11.099	21.871	33.223	42.392	62.163	
	30	6.113	16.928	34.599	49.362	53.301	67.994	
	40	6.651	22.908	40.303	57.495	55.874	67.506	
	50	8.134	24.928	48.817	53.896	64.994	69.285	

Method M-estimators** (initial vectors obtained by LMedS method)								
		position error of ICP pairs in %						
		0	10	20	30	40	50	70
% of corrupted ICP pairs	0	0.901	-	-	-	-	-	-
	5	0.917	0.952	1.058	1.384	2.250	3.412	
	10	0.955	1.044	1.985	4.989	5.170	8.145	
	20	1.281	1.813	7.074	14.730	15.965	24.256	
	30	1.978	4.515	20.087	22.944	29.150	29.808	
	40	3.125	11.830	24.686	28.721	35.876	39.737	
	50	4.383	21.759	35.840	39.807	43.349	50.821	

variations, $N_{u,r}$, for observed object distant 1 to 100 m from camera. Graph is based on data used for example in [6]: $k = l = 1643$, camera calibration error $N_c = 0,901$ pixel (the smallest error from Table I) and distance of observed object from camera is r , $r = 1, 2, \dots, 100$ meters. Camera was mounted on three meters long steel bearing structure with thermal expansion coefficient $\psi = 13 \cdot 10^{-6} K^{-1}$. If external temperature varies for $\Delta T = 40^\circ C$, then camera position changes for 1.56 mm in direction of construction vector v_s . Error N_u originated due to camera position variations decreases, by increasing distance of observed object from camera [6] (see also Fig. 4 for error N_u used in graph from Fig. 3). Similarly, a relative error ratio $N_{u,r}$ decreases (see Fig. 3). At greater distances of observed object from camera, the predominant part presents camera calibration error N_c .

Camera system on the building site is usually located some ten to hundred meters from observed objects. At such distances, the error N_u is small and practically does not influence accuracy of corresponding points estimation. For observed objects located more than 50 meters from camera, the relative error ratio $N_{u,r}$ is smaller than 5 %, with respect to the total error N (see also Fig. 3).

VI. CONCLUSION

Influence of temperature variations on calibrated camera was discussed and its ratio with respect to the total error N

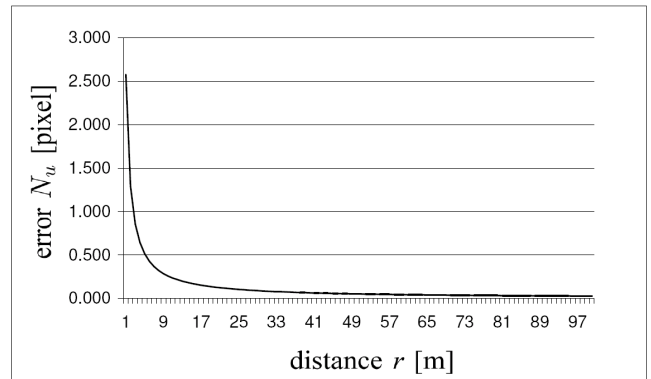


Fig. 4. Error N_u , expressed in pixels, originated due to camera position at variation of external temperature for $\Delta T = 40^\circ C$. Steel bearing structure for camera mounting is three meters long.

of calibrated cameras was determined in this paper. Error N is provoked by (i) numerical error of calibration method, (ii) inaccurate position of ICP points, and (iii) camera parameters alternations due to temperature variations. Error of calibration method (i.e. error combined from (i) and (ii)) was determined experimentally, because pre-determinate equation system for solution of fundamental matrix does not allow its analytical derivation.

Camera parameters change also due to temperature vari-

ations. In this way provoked error decreases by increasing distance of observed object from camera [6]. Analytically determined error because of camera parameters variations, N_u , and experimentally estimated camera calibration method error, N_c , was combined into total error N of calibrated cameras. Relative error ratio N_{u_r} , originated due to camera parameters variations provoked by external temperature change, decreases exponentially with distance of observed object from a camera. Thus, a contribution of error N_u , is for objects at distance more than 50 meters from camera smaller than one pixel.

Božidar Potočnik Božidar Potočnik, born in 1972, received the Doctor of Science degree in 2000 from the University of Maribor. He currently holds a position of Associate Professor in the Faculty of Electrical Engineering and Computer Science, Maribor. His research interests are segmentation algorithms at computer image processing, pattern recognition, biomedicine, cognitive vision, and machine learning. He is a member of IEEE Computer Society, IEEE Society of Engineering in Medicine and Biology, and Slovenian Pattern Recognition Society.

REFERENCES

- [1] David A. Forsyth and Jean Ponce. *Computer Vision - A Modern Approach*. Prentice Hall, August 2002. 693 pp.
- [2] Richard Hartley and Andrew Zisserman. *Multiple View Geometry in Computer Vision*. Cambridge University Press and ISBN: 0521540518, second edition, 2004.
- [3] Richard I. Hartley. In defense of the eight-point algorithm. *IEEE Transactions on pattern analysis and machine intelligence*, 19(6):580–593, June 1997.
- [4] Timo Kahlmann, Fabio Remondino, and H. Ingensand. Calibration for increased accuracy of the range imaging camera swissrangerTM. In *SPRS Commission V Symposium 'Image Engineering and Vision Metrology'*, volume XXXVI, pages 136–141, Dresden, 25-27 September 2006.
- [5] Jeffrey C. Lagarias, James A. Reeds, Margaret H. Wright, and Paul E. Wright. Convergence properties of the Nelder Mead simplex method in low dimensions. *SIAM Journal of Optimization*, 9(1):112–147, 1998.
- [6] Peter Podbreznik and Božidar Potočnik. Analytical camera model supplemented with influence of temperature variations. In *CVISP 2008 Conference, submitted*, Prague, Czech Republic, July 2008.
- [7] Peter Podbreznik and Danijel Rebolj. Automatic comparison of site images and the 4D model of the building. In Scherer Raimar J., Katranuschkov Peter, and Schapke Sven-Eric, editors, *CIB W78 22nd conference on information technology in construction*, pages 235–239, Dresden, Germany, July 2005. Institute for Construction Informatics and Technische Universität Dresden.
- [8] Peter Podbreznik and Danijel Rebolj. Building elements recognition using site images and 4D model. In Hugues Rivard; Edmond Miresco and Hani Melhem, editors, *Joint international conference on computing and decision making in civil and building engineering*, page 87, Montreal, Canada, June 2006.
- [9] Thierry Sentenac, Yannick Le Maoult, Guy Rolland, and Michel Devy. Temperature correction of radiometric and geometric models for an uncooled CCD camera in the near infrared. *IEEE Transactions on instrumentation and measurement*, 52(1):46–60, February 2003.
- [10] Zhengyou Zhang. Parameter estimation techniques: A tutorial with application to conic fitting. Technical Report 2676, Institut National de Recherche en Informatique et en Automatique, October 1995.
- [11] Zhengyou Zhang. Determining the epipolar geometry and its uncertainty: A review. *International Journal of Computer Vision*, 2(27):161–198, 1998.

Peter Podbreznik Peter Podbreznik, born in 1979, received the diploma degree in 2004 from the University of Maribor. He currently holds a position of PhD student at Faculty of Electrical Engineering and Computer Science and assistant at the Faculty of Civil Engineering, Maribor. His research interests are construction information technologies, segmentation algorithms at computer image processing, pattern recognition and computer vision.